Energy Dissipation of Unsteady Wave Breaking on Currents

AIFENG YAO AND CHIN H. WU

Department of Civil and Environmental Engineering, University of Wisconsin—Madison, Madison, Wisconsin

(Manuscript received 6 October 2003, in final form 8 April 2004)

ABSTRACT

Energy dissipation for unsteady deep-water breaking in wave groups on following and opposing currents, including partial wave-blocking conditions, was investigated by detailed laboratory measurements. A range of focusing wave conditions, including current strengths, wave spectrum slopes, and breaking intensities, were examined. Observations show that weak following and opposing currents do not alter the limiting wave steepness. The kinematics of unsteady breaking can be characterized as the one without currents simply by the Doppler shift. In contrast, strong opposing currents can cause partial wave blockings that narrow the spectral frequency bandwidth and increase the mean spectral slope. Dependence of the significant spectral peak steepness on the spectral bandwidth parameter was identified, confirming threshold behavior of breaking inception of nonlinear wave group dynamics. Loss of excessive energy fluxes due to breaking was found to depend strongly on the mean spectral slope. Wave groups of a steeper spectral slope yield fewer energy losses. In addition, the spectral distribution of energy dissipation due to breaking has the following two main characteristics: (a) significant energy dissipation occurred at frequency components that were higher than the spectral peak frequency, and little energy change at the peak frequency was found; (b) below the spectral peak frequency a small energy gain was observed. The energy-gain-to-loss ratio varies with the spectral bandwidth parameter. Higher gain–loss ratios (up to 40%) were observed for breakers on strong opposing currents under the partial wave-blocking condition. Comparison and assessment of proposed and existing parameterizations for breaking-wave energy dissipation were made using the measured data. The new proposed form provides the features for addressing these two main spectral energy distribution characteristics due to breaking with and without currents.

1. Introduction

Breaking waves, widespread over the ocean surface, play an important role in air–sea interactions (Banner and Peregrine 1993; Melville 1996; Duncan 2001). Wave breaking, among other mechanisms such as bottom friction (Komen et al. 1994), wave–turbulence interaction (Tolman and Chalikov 1996; Thais and Magnaudet 1996; Teixeira and Belcher 2002), and wind attenuation (Donelan 1999; Peirson et al. 2003), is also believed to be a dominant dissipative process for ocean wave evolution. In the field, wave breaking tends to be unsteady (Melville 1994) and more often appears in wave groups (Donelan et al. 1972; Holthuijsen and Herbers 1986). In addition, waves rarely break without the presence of currents, which may be driven by wind forcing (Banner and Phillips 1974), oceanic circulation, stratification (Peregrine 1976), or preceding surface-breaking waves (Terray et al. 1996; Melsom 1996). Therefore, better understanding and quantification of energy dissipation due to wave breaking in the presence of currents is crucial to sea-state wind–wave forecasting (Komen et al. 1994; Ris and Holthuijsen 1996). The objective of this paper is to examine the spectral distribution and energy losses of unsteady wave breaking on currents.

Over the years good progress on wind-wave modeling has been made (Hasselmann 1974; Komen et al. 1984; Phillips 1984, 1985; Resio 1987; Tolman and Chalikov 1996; Booij et al. 1999; Schneggenburger et al. 2000). Specifically, the parameterization of wave energy dissipation was improved by taking into account wave-breaking formation in wave group dynamics (Dold and Peregrine 1986; Donelan and Yuan 1994; Banner and Tian 1998; Banner et al. 2000, 2002). In a recent remarkable paper, Henrique et al. (2003) proposed a saturation-based spectral energy dissipation formula by incorporating the threshold behavior of breaking onset associated with nonlinear wave group modulation. The inclusion of an integrated spectral steepness parameter offers the flexibility of computing enhanced dissipation rates for long wave–short wave and wave–turbulence interactions. Their proposed spectral formulation dramatically improves the prediction of spectral quantities and spectral shape in fetch-limited wave conditions. On the other hand, for breaking in the presence of currents, limited information on the quantification of energy dissipation impeded our modeling progress (Ris and Holt-

Corresponding author address: Chin H. Wu, Dept. of Civil and Environmental Engineering, University of Wisconsin—Madison, Madison, WI 53706.
E-mail: chinwu@engr.wisc.edu

huijsen 1996; Smith and Seabergh 2001). Recently, Chawla and Kirby (2002) introduced a breaking probability function based upon a wave slope criterion for quantifying energy dissipation due to current-limited wave breaking. Their spectral model, which includes breaking probability in the modified bore energy dissipation formula, reasonably simulates the spectral evolution and frequency downshifting for the wave blocking. In all of these models, the general formulation of breaking energy dissipation is exclusively parameterized as energy loss and is proportional to the spectral density. Consequently, breaking leads to energy sinks across the entire wave spectrum and the largest dissipation occurs at the spectral peak.

Detailed laboratory experiments have revealed some characteristics of energy dissipation due to wave breaking. These experiments range from steady wave breaking (Duncan 1981), unsteady wave breaking generated by temporal and spatial linear superposition wave focusing or dispersive focusing (Rapp and Melville 1990; Kway et al. 1998; Meza et al. 2000), geometric and dispersive focusing (Nepf et al. 1998; Wu and Nepf 2002), nonlinear wave focusing by Benjamin–Feir instability (Waseda and Tulin 1999), to wave breaking in the presence of strong opposing currents (Lai et al. 1989; Smith and Seabergh 2001; Chawla and Kirby 1998, 2002). In general, two important features of spectral energy dissipation for unsteady breakers in wave groups have been identified. First, significant energy dissipation is found to occur at frequencies that are higher than the spectral peak frequency, while little energy is lost at the spectral peak (Rapp and Melville 1990; Kway et al. 1998; Meza et al. 2000). Second, wave frequencies below the spectral peak seem to gain a small portion of energy after breaking. For example, Waseda and Tulin (1999) found that strong breaking can irreversibly transfer energy from the higher sideband to lower sideband under a self-modulated narrow-bandwidth three-wave group. For breaking waves generated from the dispersive focusing, several observations (Rapp and Melville 1990; Nepf et al. 1998; Meza et al. 2000) showed that a small amount of energy was gained below the spectral peak, which may be due to the ''maser'' mechanism (Longuet-Higgins 1969), the change in the gradient of radiation stress accompanying breaking (Melville 1996), or momentum loss of wave breaking transferring to the mean currents (Rapp and Melville 1990; Melsom 1996). Nevertheless, the two identified features are contradictory to the existing parameterization of wave energy dissipation.

Losses of excess energy/momentum fluxes (Melville and Rapp 1985) were used to quantify the amount of dissipation for different types of unsteady breakers. A number of investigations have reported energy losses for a single, unsteady breaker in the wave groups (Rapp and Melville 1990; Lammare 1993; Kway et al. 1998; Nepf et al. 1998). A variety of reported energy losses were summarized in Wu and Nepf (2002). For example, a violent plunging breaker can result in energy loss from 14% to 40%. Dimensionality of the wave field may explain the dramatic variation in energy loss (She et al. 1997; Wu and Nepf 2002). Kway et al. (1998) argued that the variation of energy losses for even a two-dimensional breaker is caused by the differences of the input wave spectra slopes. Note that all the above experiments were conducted in the absence of currents. For random breaking waves on strong opposing currents with or without blocking, an even wider range of energy losses, for example, 5%–50% (Chawla and Kirby 2002) and 20%–60% (Smith and Seabergh 2001), was reported. While these differences could be attributed to the breaking intensities, occurrence probabilities, or background turbulences, difficulties in reconciling these results in the literature remain.

This study is motivated by the relative shortage of studies of unsteady wave breaking on currents, some unsolved discrepancy on energy dissipation, and the gap between the existing parameterizations of energy dissipation and experimental observations. To address these issues, we investigate breaking energy dissipation in wave groups on currents in a well-controlled two-dimensional laboratory flume. Experimental cases with varying current strengths, wave spectrum slopes, and breaking intensities are examined. Several parameters, including spectrum-based wave steepness, frequency bandwidth, and mean spectral slope, were employed to examine breaking onset and dissipation. We believe that this experimental study can provide new insight on energy dissipation through breaking and help to clarify some unsolved questions.

Following the introduction in section 1, the remainder of this paper is organized as follows. In section 2, the experimental approach is described, with emphasis on the generation of breaking on currents and data analysis. In section 3, the experimental results are presented, including the evolution of surface displacement, losses of excess energy flux, variation of wave energy spectra, and spectral distribution of energy dissipation. Parameterization of energy dissipation due to wave breaking is discussed in section 4. Last, summaries and recommendations are given in section 5.

2. Experimental approach

a. Experimental facility and instrumentation

The experiments were conducted in a wave–current flume in the Environmental Fluid Mechanics Laboratory at the University of Wisconsin—Madison (Fig. 1). The flume is 46 m long, 0.90 m wide, and filled with a water depth of $d = 0.60$ m. A coordinate system is defined at the free surface and the z axis is vertically upward. The x axis is in the direction of wave propagation with the starting position at the bottom-hinged wave maker. The wave-maker motion was controlled by a linear servomechanism amplifier fed by voltage signals via an

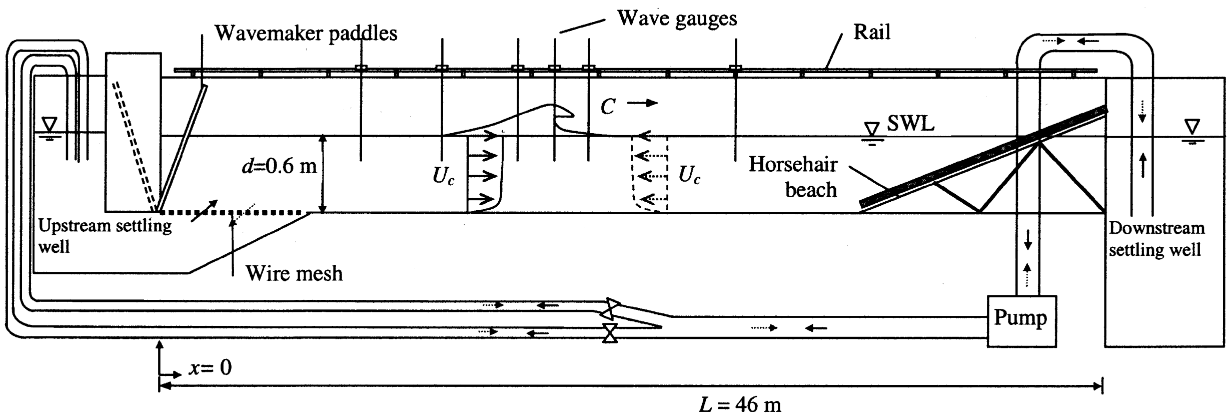

FIG. 1. Schematic of the experimental setup. The wave–current flume consists of a flat-paddle wave maker, a sloping opening with a wired mesh, a leveled bottom, an absorption beach, a recirculating pipeline, and a bidirectional pump.

AT-AO-6 data acquisition board (National Instruments Corp., Austin, Texas) on a Pentium 133–powered master computer. At the other end of the flume, a passive absorption wooden frame beach, covered with 4-in.-thick porous horsehair mats, at a slope of 1:10, was installed. The beach was found to absorb 97% of the monochromatic wave energy, based on the three-gauge method (Rosengaus-Moshinsky 1987).

Recirculation currents were introduced by a bidirectional centrifugal pump that drew water from a settling well at one end of the flume to another settling well at the other end through stainless steel spiral pipes. Following currents, moving in the same direction as wave propagation, were achieved by a sloping bed opening covered with a wire mesh in front of the wave maker. By reversing the pump the water can go through the beach to generate opposing currents. A microacoustic Doppler velocimeter (16 MHz, SonTek/YSI, Inc., San Diego, California) with a specified accuracy up to 0.3 cm s^{-1} was employed to measure the velocity profile of both following and opposing current conditions. Detailed measurements of the vertical current profile were carried out from $x = 6$ m to $x = 14$ m along the centerline of the flume. Figure 2 shows the mean current profiles averaged over 600 s (15 000 samples). Positive (negative) values represent the following (opposing) currents. Essentially uniform current profiles were found about 30 cm below the surface, corresponding to approximately 3 times the typical maximum wave height in this experiment. While slight shear was observed near the flume bottom, it was deemed unlikely to interact with deep-water surface waves here. The maximum streamwise variations of the mean velocity profiles were measured to be less than 5% between $x = 4$ m and $x = 16$ m. The maximum turbulence intensity was estimated to be less than 15% using the ensemble average of the 15 000 samples. Therefore, the surface waves were considered to travel on the uniform currents.

Six capacitance-type wave gauges, manufactured by Protecno S. R. L. (Noventa Padovana, Italy), were used to measure the water surface displacement at a spatial interval of 0.20 m using a movable carriage system. The penetrated wave wire has only a diameter of 3 mm so that the disturbance (or fluctuation) of the existence of wave gages under the current flow condition was measured to be less than 1 mm. Surface displacement data were recorded at 51–76 positions, depending on the measurement span of the testing case. A Pentium 90–powered computer with the 12-bit data acquisition board (DAS1602, Keithley Instruments, Inc., Cleveland, Ohio) was used to record surface displacement data at 200 Hz. For wave breaking in the presence of currents, the desired current was generated first and elapsed at least 1 h for achieving a steady-state water level, which was used as a zero reference water level for calibrating the wave gages. The accuracy of the wave gauges is 0.5 mm through the calibration.

b. *Breaking wave generation on currents*

Both wave–wave and wave–current interactions are believed to be important mechanisms for unsteady wave breaking or large-scale whitecapping in oceans (Longuet-Higgins and Stewart 1960; Benjamin and Feir 1967; Kjeldsen and Myrhaug 1979; Phillips 1977). The spatial and temporal linear superposition of focusing wave components due to their frequency dispersion has been widely used in laboratory settings to generate an individual breaking wave within a wave group to mimic transient wave breaking in the oceans (Rapp and Melville 1990; Kway et al. 1998; Wu and Nepf 2002). The advantage of the frequency-focusing technique is its capability to generate a repeatable, isolated, single breaker within a dispersive wave train. In the present study, unlike generating irregular random waves on opposing currents (Hedges et al. 1985; Suh et al. 1994, 2000; Chawla and Kirby 2002), we extend the spatial and temporal focusing method by further accounting for wave–current interactions. The intrinsic frequency σ on a current U is related to the apparent frequency ω and

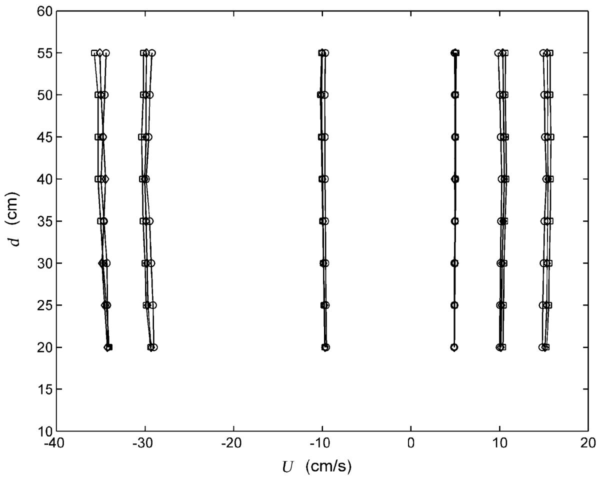

FIG. 2. Measured velocity profiles of both following and opposing currents considered in this study at 6 (circle), 10 (diamond), and 14 (square) m downstream of the wave maker.

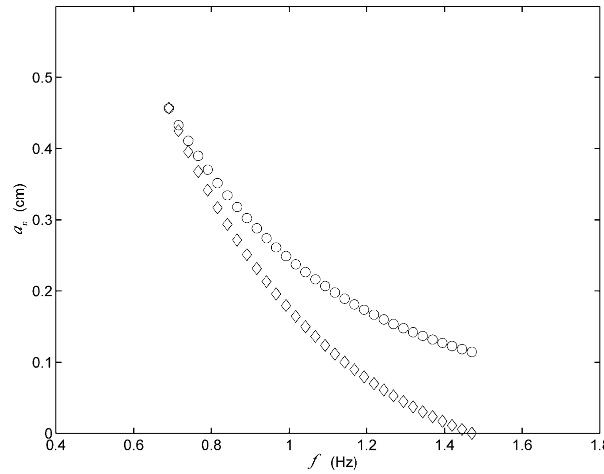

FIG. 3. Input wave amplitude spectra: constant steepness (circle) and linear steepness (diamond) spectra.

the corresponding wavenumber k through the linear Doppler-shifted dispersion relation (Peregrine 1976)

$$\sigma^2 = (\omega - kU)^2 = kg \tanh(kd), \tag{1}$$

where g is the gravitational constant. If a wave propagates in the same direction as the current, the Doppler's effect in Eq. (1) would result in a smaller intrinsic frequency and wavenumber of the wave. The opposite is true, except for the wave-blocking condition (Huang et al. 1972; Lai et al. 1989).

Based upon the linear wave theory, the free surface displacement for generating a dispersive wave packet on a current at the paddle is described as

$$\eta(x = 0, t) = \sum_{n=1}^{N=32} a_n \cos(k_n x_f - \omega_n t + \phi_n), \tag{2}$$

where a_n is the amplitude of nth wave component, $N = 32$ is the total number of wave components, and ϕ_n is the required phase shift to ensure that all of the wave components occur at the theoretical focusing location x_f at the focusing time t_f, that is,

$$\phi_n = k_n x_f - \omega_n t_f + 2\pi m \ (m = 0, \pm 1, \pm 2, \ldots). \tag{3}$$

On the condition of wave blocking due to strong opposing currents, there is no real solution for high-frequency wave components in Eq. (1). Therefore, the phase for those components cannot be determined. To overcome this difficulty, random phases for high-frequency components were assigned. From numerical simulations of spatially and temporally focusing ''deterministic'' wave components on ''random'' wave components, Pelinovsky and Kharif (2000) and Slunyaev et al. (2002) showed that a random phase wave field would not prevent the focusing phenomenon.

The amplitude of each wave component in Eq. (2) was determined based upon a constant steepness spectrum (Lamerre 1993; Nepf et al. 1998)

$$a_n = \frac{G_1}{k_n^0} \tag{4}$$

and a linear steepness spectrum

$$a_n = \frac{k_N^0 - k_n^0}{k_n^0(k_N^0 - k_1^0)} G_2, \tag{5}$$

where the superscript ''0'' corresponds to zero current, and G_1 and G_2 are the gain factors for varying the overall intensity of breaker. Figure 3 depicts a representative constant steepness wave spectrum and a linear steepness wave spectrum over the input frequency range 0.69–1.47 Hz. Other wave spectral distributions, for example, a constant-amplitude spectrum (Rapp and Melville 1990) and the Pierson–Moskowitz spectrum (Kway et al. 1998), were also tested. It was found that the wave group based upon the linear or constant steepness wave spectrum is more capable of creating a single unsteady breaker without the occurrence of unmature breakings. In particular, the linear steepness spectrum can result in a better breaker on currents.

Last, the wave packet propagating in the presence of currents can be described by the following parameters:

$$\eta k_c = \Psi\left(x_f k_c, \frac{\Delta\omega}{\omega_c}, dk_c, Ak_c, \frac{U}{C}\right), \tag{6}$$

where k_c is the central wavenumber of the wave packet corresponding to the input central wave frequency $f_c = (0.69 + 1.47)/2 = 1.08$ Hz. A frequency bandwidth ratio $\Delta\omega/\omega_c = \Delta f/f_c = 0.73$ was chosen for all of the experimental conditions. A relative water depth dk_c was prescribed as in the deep-water regime. An input spectrum-based steepness was given by Ak_c (Rapp and Melville 1990), where $A = \sum_{n=1}^{N} a_n$. The ratio U/C defines

TABLE 1. Experimental cases.

Case	Input wave spectrum ($a_n k_n$)	Frequency bandwidth $\Delta f/f_c$	Intrinsic frequency range σ* (Hz)	Current velocity U (cm s^{-1})
1	Constant	0.73	0.69–1.47	0
2	Constant	0.73	0.66–1.43	5
3	Constant	0.73	0.65–1.36	10
4	Constant	0.73	0.63–1.35	15
5	Constant	0.73	0.70–1.55	−5
6	Linear	0.73	0.69–1.47	0
7	Linear	0.73	0.65–1.36	10
8	Linear	0.73	0.72–1.65	−10
9	Linear	0.73	0.82–2.44**	−30
10	Linear	0.73	0.86–1.91**	−35

* Intrinsic frequency range is calculated using Eq. (1).
** Wave-blocking condition.

the relative strength of a coexisting current (Thomas and Klopman 1997), where $C = \omega_c/k_c = 1.44$ m s^{-1} is the characteristic wave phase speed. In this study, both parameters Ak_c and U/C were varied to generate the highest nonbreaking wave through weak-to-strong breakers, named as incipient, spilling, and plunging waves (Rapp and Melville 1990) on both following and opposing currents. All experimental cases are listed in Table 1. Overall, these breaking waves were generated based upon the temporal and spatial linear wave in-phase superposition of all the frequency components at the focal time and position, which finally exceeded the threshold of nonlinear waves. Note that it is recognized that the Benjamin–Feir instability or nonlinear focusing can also lead to steep and breaking waves for wave trains with narrow-frequency bandwidths (Melville 1982; Waseda and Tulin 1999). Alber (1978) suggested that the Benjamin–Feir instability is able to act in a unidirectional wave train if $\Delta f/f_c$ is less than the average wave steepness. For the partial wave-blocking cases 9 and 10, the estimated frequency bandwidth was 0.61 and 0.46, respectively, which are still higher than their corresponding average wave steepness. Therefore, the mechanism of Benjamin–Feir instability is not believed to be significant in this experiment.

c. Data analysis

1) LOSSES OF EXCESS ENERGY FLUXES

Under no-current conditions, the control volume approach based upon the wave energy conservation equation has been used to estimate energy losses for two-dimensional (Rapp and Melville 1990) and three-dimensional (Wu and Nepf 2002) breaking. In this study we extended the method to the condition where both waves and currents exist. Following Phillips (1977) and Jonsson (1990), the depth-integrated and time-averaged conservation equations for energy in a two-dimensional wave–current-leveled flume can be described as

$$\frac{\partial E}{\partial t} + \frac{\partial F}{\partial x} = -E_d, \tag{7}$$

where $E = (1/2)\rho h U^2 + E_w$ is the total energy density and E_w is the wave energy density; $F = (1/2)\rho d U^3 + E_w(c_g + U) + S_{xx}U$ is the total energy flux and c_g is the intrinsic wave group velocity; $S_{xx} = 1/2E_w$ is the radiation stress for the deep water; and E_d is the total energy dissipation due to viscous dissipation, wave attenuation on a current, wave blocking, and breaking.

The evaluation of Eq. (7) requires detailed temporal and spatial measurements of velocity and pressure fields as well as surface displacement. We simplify the estimate by the following experimental conditions: (i) a steady volumetric flow rate was assured by a constant pumping system so that either the combined wave–current motion was in a steady state or there was no wave-induced net flow (Jonsson 1990); (ii) the spatial variation of the mean horizontal velocity along the x direction was less than 5%, giving $U \sim$ constant; (iii) water depth variation due to wave- and current-induced set down was negligible, which is justified by the set down (Jonsson 1990)

$$\Delta h = \frac{U^2}{2g} - \frac{H^2}{8hc}U, \tag{8}$$

where c is the intrinsic wave speed (The maximum set down within all the experimental cases was estimated to be less than 3 mm, which was 0.5% of the water depth. Therefore, the water depth can be regarded as a constant); and (iv) away from the focusing location, most waves are, at most, weakly nonlinear. Therefore, the equipartition of kinetic and potential energy of wave motion and a constant wave group speed were valid. With these conditions, by integrating Eq. (7) over time and within the control volume bounded by the entire water depth, an upstream boundary, and a downstream boundary far away from the breaking point (Rapp and Melville 1990; Nepf et al. 1998), the normalized loss in the excess energy flux is

$$\frac{\Delta\overline{F}}{\overline{F}_0} = \frac{\overline{(\Delta E_w)(c_g + 3/2U)}}{\overline{(E_w)_0(c_g + 3/2U)}} = \frac{\Delta\overline{\eta^2}}{\overline{\eta_0^2}}, \tag{9}$$

where the subscript 0 denotes quantity at the upstream boundary of the control volume, the overbar represents a long time integration for the whole wave packet, and $\overline{\eta^2}$ is the surface displacement variance, defined as

$$\overline{\eta^2} = \frac{1}{T_0}\int_0^{T_0} \eta^2\, dt, \tag{10}$$

where the integration time $T_0 = N/\Delta f = 40 \sim 70$ s. A smaller Δf was used in the case of wave blocking. The T_0 was chosen to be long enough to capture the passage of the wave packet at all measurement positions and to be less than the elapsed time when the energetic reflection waves arrived. Energy losses for spilling and plunging waves were estimated by subtracting those of incipient waves for the purpose of obtaining energy losses exclusively from breaking.

2) Spectral analysis

Spectral evolution for a nonlinear wave packet was used to reveal the dynamics of wave–wave interaction and wave-breaking processes (Rapp and Melville 1990; Baldock et al. 1996; Nepf et al. 1998; Meza et al. 2000). In this study, wave energy density spectra were estimated from the time series of surface displacements using the fast Fourier transform (FFT) using 10 000–14 000 points with a three-point moving average filter. For different current conditions, the total sampling time was between 50 and 70 s, giving a frequency resolution of 0.02–0.014 Hz.

Spectral energy dissipation due to breaking can be determined by comparing the spectra measured before and after breaking (Rapp and Melville 1990; Kway et al. 1998; Nepf et al. 1998). Variations of wave spectra in a wave train along the wave propagation in a flume could be attributed to nonlinear wave–wave interactions (Baldock et al. 1996), viscous dissipation, wave attenuation on a current, strong opposing current blocking, and wave breaking. To estimate the spectral changes exclusively due to breaking events, the following procedures were adopted. First, to minimize energy density variations at both high- and low-frequency ranges due to nonlinear wave–wave interaction or bound wave effects, wave spectra at an upstream and a downstream reference positions, far away from the breaking point, were chosen. Second, the difference of wave spectra before and after breaking was normalized with the spectral peak at the upstream reference position. A similar procedure was applied to an incipient wave for estimating energy loss due to viscous dissipation, wave attenuation, and wave blocking. Third, normalized wave spectral differences due to spillers and plungers were calculated by subtracting those of incipient waves to obtain energy losses exclusively for wave breaking. Fourth, representative statistics were achieved by ensemble averaging of wave spectra from repeatable experimental runs under identical wave–current conditions.

3) Parameters for wave groups

To characterize the dynamics of nonlinear wave groups, a number of parameters have been proposed in the literature. These parameters, including carrier wave steepness (Dold and Peregrine 1986), significant wave steepness (Huang 1986), spectrum-based global steepness (Rapp and Melville 1990), nondimensional energy and momentum growth rates (Banner and Tian 1998), and significant spectral peak steepness (Banner et al. 2000), have been related to directionality (Su et al. 1982; She et al. 1997; Nepf et al. 1998), wave spectrum slope (Kway et al. 1998), and spectral bandwidth (Baldock et al. 1996; Brown and Jensen 2001) for characterizing nonlinearity of a wave group leading to wave breaking.

In this study, in addition to the frequency bandwidth ratio $\Delta\omega/\omega_c = \Delta f/f_c$, we used the spectral bandwidth parameter (Longuet-Higgins 1984), defined as

$$\upsilon = \sqrt{m_2 m_0/m_1^2 - 1}, \tag{11}$$

where m_i is the ith spectral moment, given by

$$m_i = \int_0^\infty \omega^i S(\omega)\, d\omega. \tag{12}$$

A bandpass filtering with upper and lower cutoffs at $1.5f_p$ and $0.5f_p$ was usually suggested, where f_p is the peak spectral frequency. Here, the input frequency range 0.69–1.47 Hz was used. Smaller upper cutoff frequencies were used for wave-blocking cases based on theoretical estimates.

The significant spectral peak steepness, a good indicator of wave group nonlinearity (Banner et al. 2000), is defined as

$$\varepsilon_p = \frac{H_s k_p}{2}, \tag{13}$$

where $H_s = 4[\int_0^\infty S(f)\, df]^{1/2}$ is the significant wave height based upon the wave density spectrum $S(f)$, and k_p is the peak wavenumber corresponding to f_p. To calculate ε_p for all experimental cases, the wave spectra at the upstream reference position were used. The same cutoff frequencies, as used to estimate υ, were used to calculate the significant wave height.

3. Experimental results

a. Surface displacement

Figure 4 depicts the temporal and spatial evolutions of the free surface displacements for three incipient wave trains on following, opposing, and zero currents. The label on the left side of each plot marks the distance with respect to the same theoretical focal point x_f. Because the wave train on the opposing current traveled slower than those on the zero and following currents, the wave train on the opposing current was released earlier than those on zero and following currents. With wave–current interactions and a dispersive process, this arrangement ensured that all the frequency components of three wave trains were in phase at the predetermined, theoretical focal location, that is, $x^* = x - x_f = 0$ m. Because of nonlinearity, the actual position of maximum wave amplitude was not at the theoretical focal location prescribed by the linear wave theory (Baldock et al. 1996), but occurred approximately at $x^* = 1$ m. After that, the three wave trains became out of phase, with the following current leading, followed by a wave train on the zero current and then the opposing current. This result is consistent with the Doppler shift effect in Eq. (1). Using the data analysis technique described in Wu

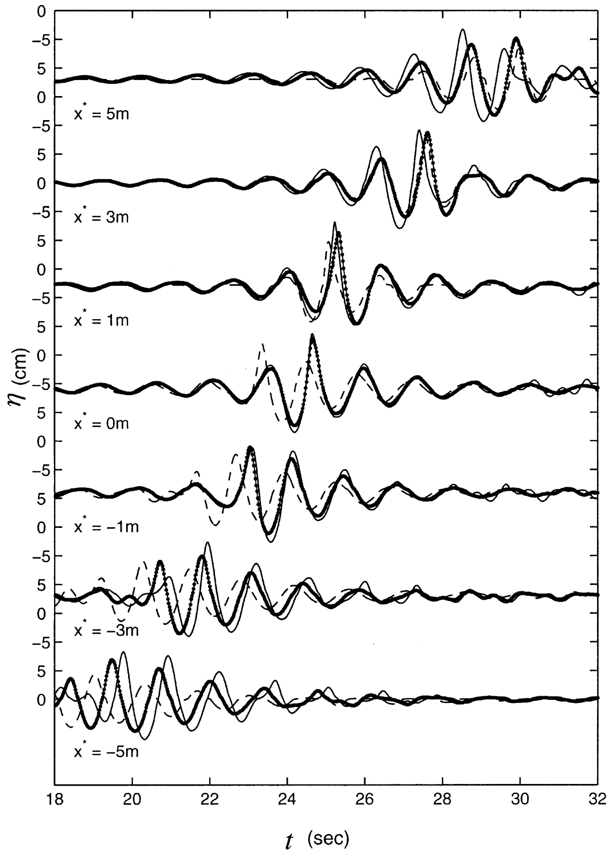

FIG. 4. Evolution of surface displacement for the incipient waves based upon the linear steepness spectra; a zero current (case 6; dots), the following current $U = 10$ cm s^{-1} (case 7; solid lines), and the opposing current $U = -10$ cm s^{-1} (case 8; dashed lines).

and Nepf (2002), the maximum local wave steepness, that is, the ratio of the maximum wave height to the wavelength, of the three wave trains was found to be constant, that is, $H/L = 0.080 \pm 0.001$ (or $ak = 0.250 \pm 0.003$).

The temporal and spatial evolutions of the spilling and plunging breakers on the following, opposing, and zero currents are shown in Figs. 5a and 5b. The spilling breakers occurred after the theoretical focal point, that is, $x^* = 0.4$, 0.6, and 0.8 m on the opposing, zero, and following currents, respectively. Initiating at the wave crest preceding the spillers, the plunging breakers occurred ahead of the theoretical focal point, that is, $x^* = -1.2$, -1.4, and -1.6 m on the opposing, zero, and following currents, respectively. The separation distance between the spiller and the plunger is approximately one wavelength of the wave train (Rapp and Melville 1990; Kway et al. 1998; Nepf et al. 1998). A larger separation distance on the following current was observed due to the current modulation that lengthens the wavelength. In addition, a higher maximum wave crest was observed on the following current. However, the local wave steepness, that is, the ratio of the maximum wave height to the wavelength, of a wave train on a uniform current remained constant at $H/L = 0.081 \pm 0.001$ (or $ak = 0.255 \pm 0.003$) for spilling breakers and $H/L = 0.097 \pm 0.002$ (or $ak = 0.304 \pm 0.005$) for plunging breakers. These results suggest that the kinematics of unsteady breakings on weak and uniform currents can be characterized as breakings without currents simply by the Doppler effect.

Figure 6 shows the surface displacement time histories for a spilling breaker on the strong opposing -30 cm s^{-1} current. Before the focusing point, the higher-frequency components with random phases appeared in the surface displacements. The strong opposing current acted as a low-pass filter to block some higher-frequency waves (Jonsson 1990). The remaining unblocked lower-frequency waves underwent the dispersive process to focus at $x^* = 3$ m, confirming that the random phase wave field would not prevent the focusing phenomenon (Pelinovsky and Kharif 2000; Slunyaev et al. 2002). The location of the spilling crest occurred farther away from the theoretical focal point, which may result from the increased nonlinearity due to a narrower frequency bandwidth (Baldock et al. 1996). In addition, the local wave steepness was elevated to $H/L = 0.103 \pm 0.003$ (or $ak_b = 0.351 \pm 0.003$) for the spilling breaker. Similar characteristics were found for the plunging breaker on the strong opposing currents with a higher wave steepness at $H/L = 0.115 \pm 0.004$ (or $ak_b = 0.391 \pm 0.003$), occurred about one wavelength upstream of the spilling breaker. The results indicate that strong opposing currents induced partial spectral wave blocking that can alter the kinematics of breaking characteristics, in particular, the limiting wave steepness.

b. Energy losses

Figures 7a–7c show the spatial evolution of the normalized variance of the surface displacement, that is, excess energy fluxes, for the incipient, spilling, and plunging waves on 10, -5, and -35 cm s^{-1} currents. For the following current in Fig. 7a, approximately 5% viscous decay was observed in the nonbreaking incipient wave. Higher energy decay, approximately 10%, was found on the incipient wave on an opposing current shown in Fig. 7b, reflecting greater attenuation on an opposing current than that on a following current. On a stronger opposing current in Fig. 7c, much higher energy decay was observed, which may be due to wave blocking (Smith and Seabergh 2001; Chawla and Kirby 2002) or due to an increase of the limiting wave steepness. Interestingly, wave decay was enhanced in the vicinity of the focused incipient steep waves, that is, $(x - x_f)k_c \approx -5 \sim 5$ in Fig. 7b and $(x - x_f)k_c \approx 30 \sim 60$ in Fig. 7c, than those before and beyond this region, suggesting that wave steepness can play some role in attenuating wave energy. Dependence of wave decay on wave steepness has been experimentally revealed in Kemp and Simons (1982, 1983) and corroborated in

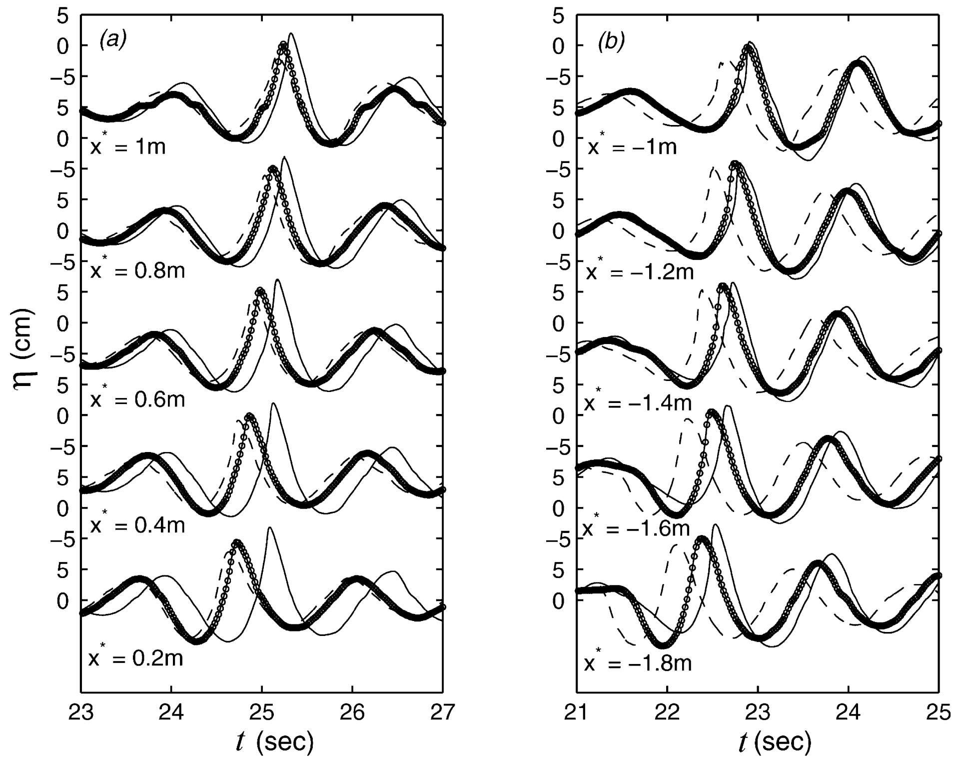

FIG. 5. Same as in Fig. 4, but for (a) spiller and (b) plunger.

Thais et al. (2001). Enhanced wave attenuation due to the opposing wind-induced wave steepness increase was also shown by Donelan (1999) and Peirson et al. (2003).

In reference to the nonbreaking incipient waves, the energy losses for spillers and plungers were estimated and listed in Table 2. For a constant steepness wave spectrum (cases 1–5), the spilling and plunging breakers, with or without currents, lost about 6% and 16% of their original energy. Smaller energy losses (i.e., 4% and 12%) for the spilling and plunging breakers with a linear steepness wave spectrum were observed in the weak current cases 6–8. The wave group with a flatter wave spectrum slope, for example, the constant steepness spectrum, was found to have higher energy losses than those of the linear steepness spectrum, consistent with the qualitative trend observed by Kway et al. (1998) for the constant amplitude, Pierson–Moskowitz, and constant steepness spectrums. This trend also confirms the statement that the most energy loss in breaking is from the high-frequency tail of the spectrum (Rapp and Melville 1990).

In this study, we proposed a mean spectral slope $\overline{dS^*/df^*} = 1/M \sum_{m=1}^{M} dS_m^*/df^*$ to quantify the spectral shape listed in Table 2. Note that $S^*(f^*) = Sf_c/E$ is the normalized input spectrum with a normalized frequency $f^* = f/f_c$. For the same frequency bandwidth, $\Delta f/f_c = 0.73$, in Rapp and Melville (1990) and our experiments, the wave group with a milder slope, that is, a constant amplitude spectrum, results in larger breaking energy losses. For different frequency bandwidths, that is, $\Delta f/f_c = 0.65$ in Kway et al. (1998) and $\Delta f/f_c = 1$ in Larmarre (1993), the wave breaking with milder $\overline{dS^*/df^*}$ were also found to have larger energy losses. In contrast, the wave groups that are partially blocked by strong opposing currents in cases 9 and 10 result in steeper $\overline{dS^*/df^*}$. Consequently, less energy losses were observed. For example, only a 3% loss for spillers and 6% for plungers on a -35 cm s^{-1} strong opposing current were found. Figure 8 shows that there is a strong dependence of wave-breaking energy losses on $\overline{dS^*/df^*}$, revealed from our experimental cases and previous results. To the best of our knowledge, the relationship between mean slope $\overline{dS^*/df^*}$ and energy losses for unsteady breakers in focused wave groups has not been revealed before. Finally, it will be very valuable to further examine the proposed mean spectral slope $\overline{dS^*/df^*}$ and energy losses in field (rather than laboratory) experiments.

c. Spectral evolution

Energy density spectra of the recorded surface displacements, estimated by the FFT technique described in section 2c(2), were used to investigate energy redistribution of a wave evolution. Figures 9a and 9b show the energy density spectra at various positions for the incipient waves on a 10 cm s^{-1} following current and a -10 cm s^{-1} weak opposing current, respectively. The

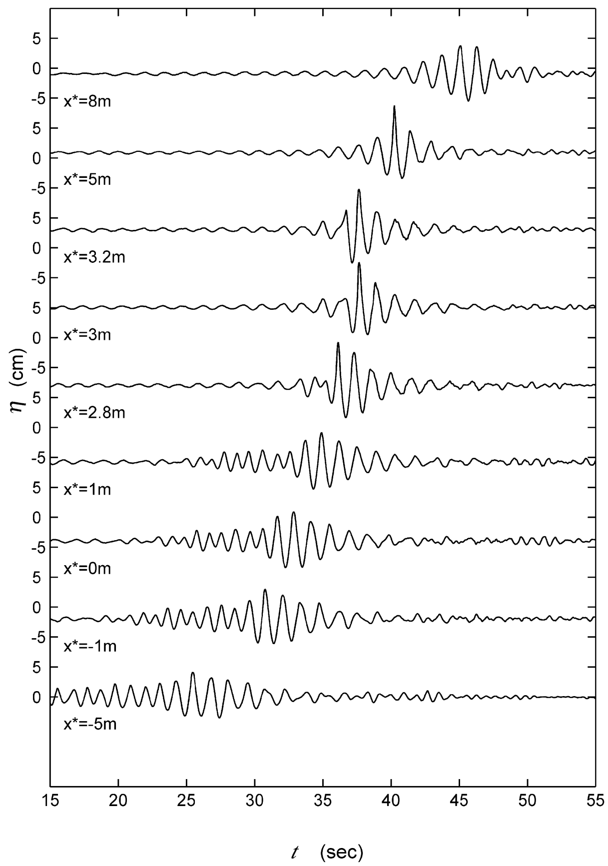

FIG. 6. Evolution of surface displacement for the spiller on a strong opposing current $U = -30$ cm s^{-1} with wave blocking in case 9.

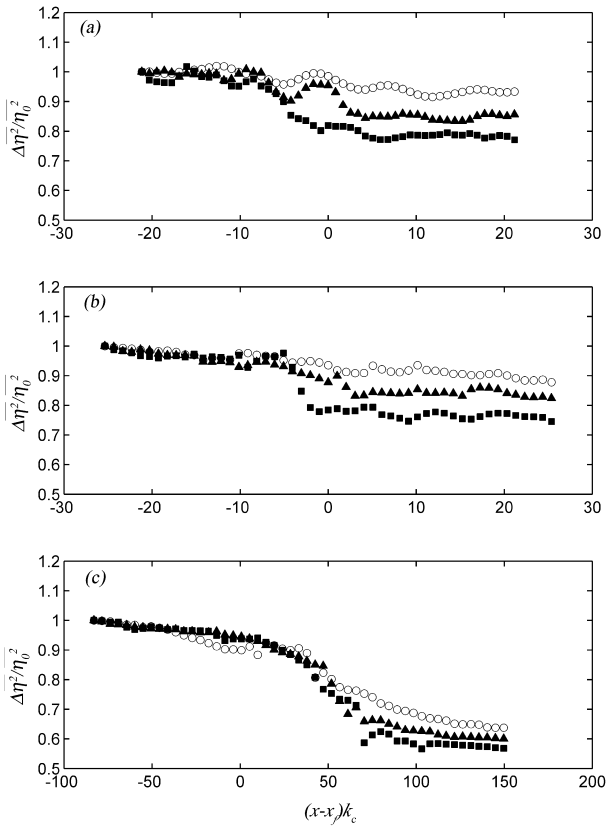

FIG. 7. Loss of excess energy fluxes of the incipient wave (open circles), spiller (triangles), and plunger (squares) on (a) a following current $U = 10$ cm s^{-1} in case 3, (b) a weak opposing current $U = -5$ cm s^{-1} in case 5, and (c) a strong opposing current $U = -35$ cm s^{-1} in case 10.

TABLE 2. Loss of excess energy flux.

2D experiment		Input spectrum: Spectrum-type frequency bandwidth	Input spectrum: Mean slope* dS^*/df^*	Spilling breaker (%)	Plunging breaker
Present study	Case 1	$a_n k_n$ = constant = G_1, $\Delta f/f_c = 0.73$, $f_c = 1.08$ Hz	−6.89	7	14
	Case 2			7	15
	Case 3			8	15
	Case 4			8	14
	Case 5			7	15
	Case 6	$a_n k_n$ = linear, $\Delta f/f_c = 0.73$, $f_c = 1.08$ Hz	−10.95	4	11
	Case 7			5	13
	Case 8			4	10
	Case 9	$a_n k_n$ = linear, $\Delta f/f_c = 0.73$, $f_c = 1.08$ Hz	−13.91**	4	9
	Case 10	$a_n k_n$ = linear, $\Delta f/f_c = 0.73$, $f_c = 1.08$ Hz	−19.78**	3	6
Rapp and Melville (1990)		$a_n = G_1$, $\Delta f/f_c = 0.73$, $f_c = 0.88$ Hz	0	10	24
		$a_n = G_1$, $\Delta f/f_c = 0.73$, $f_c = 1.08$ Hz		10	20
		$a_n = G_1$, $\Delta f/f_c = 0.73$, $f_c = 1.28$ Hz		10	25
Lamarre (1993)		$a_n k_n = G_1$, $\Delta f/f_c = 1.0$, $f_c = 0.88$ Hz	−7.53	8	15
Kway et al. (1998)		$a_n = G_1$, $\Delta f/f_c = 0.65$, $f_c = 0.83$ Hz	0	4	22
		$a_n k_n = G_1$, $\Delta f/f_c = 0.65$, $f_c = 0.83$ Hz	−4.90	—	14
		Pierson–Moskowitz, $\Delta f/f_c = 0.65$, $f_c = 0.83$ Hz	−3.19	—	20

* Here $S^* = Sf_c/E$ and $f^* = f/f_c$ are normalized wave density spectrum and wave frequency, respectively, where $E = 1/2a_n^2$ is the total spectral energy, and a_n is the amplitude of wave components.

** Wave-blocking case using the theoretical estimate by Mei (1983).

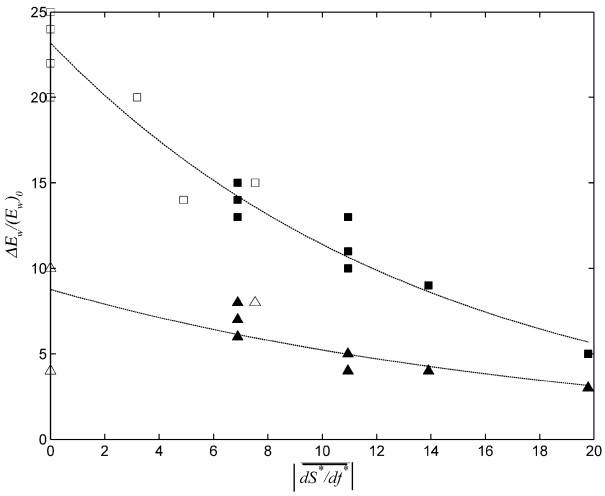

FIG. 8. Normalized energy losses $\Delta E_w/(E_w)_0$ against the absolute mean slope of input spectra $|\overline{dS^*/df^*}|$. The filled symbols are for the present experiment and the open symbols for the previously reported experiments, with squares for plungers and triangles for spillers.

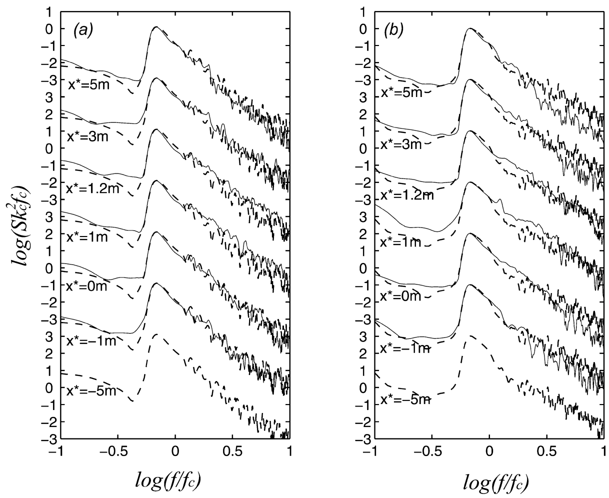

FIG. 9. Spectral evolution of the incipient waves on (a) a following current $U = -10$ cm s^{-1} in case 7 and (b) an opposing current $U = -10$ cm s^{-1} in case 8; the density spectrum at the upstream reference position (dashed lines) and the spectra at the positions labeled at the lower-left corner of each plot, $x^* = x - x_f$ with x_f the theoretical focal position (solid lines).

dashed lines represent the density spectrum at the upstream reference position, and the solid lines denote the ones at the marked positions in the plot. During the focusing process, wave–wave interactions became important and were pronounced in the vicinity of the focusing location at $x^* = 1.2$ m on both following and opposing currents. Features of energy transfer to the higher frequencies were clearly apparent, consistent with observations of incipient waves without currents by Rapp and Melville (1990), Baldock et al. (1996), and Meza et al. (2000). Beyond the focusing point, the wave packet dispersed and the effects of the wave–wave interaction gradually diminished. At $x^* = 5$ m the spectra for a nonbreaking incipient wave on a following current returned to its initial reference level, suggesting that nonlinear energy transfer is reversible, except for some viscous dissipation near the peak frequency. In contrast, for the incipient wave on the opposing current, the energy transfer to the higher frequencies did not recover to the original reference spectra. As argued by Johannessen and Swan (2001), nonlinear energy transfer in focusing wave groups cannot be fully explained by slowly resonant interactions (Hasselmann 1962; Phillips 1977) and the associated bound-wave effects (Longuett-Higgins and Stewart 1960). Instead, a rapid widening of a free-wave regime or nearly free wave components arising at the higher-frequency end of the input spectrum is more important to the formation of extremely steep waves. In Fig. 9b, the weak -10 cm s^{-1} opposing current blocked the higher frequency, that is, above $f = 10^{0.45}$, $f_c = 3.0$ Hz at $x^* = 5$ m. One should expect that the associated bound waves should not be affected by the weak opposing current because the bound-wave components would simply propagate at the speed of the associated input range of the free waves, which is not the case here. Our observations support their arguments of the existence of a locally widened free-wave regime. This finding also suggests that the dynamics of focusing unsteady waves on weak opposing currents cannot be addressed by simply changing a reference frame with the associated current.

In the case of breaking, irreversible energy spectra higher than the peak frequency before and after wave breaking were identified (Rapp and Melville 1990; Nepf et al. 1998). Figure 10a illustrates the spectral energy variation for the plunger on an opposing -10 cm s^{-1} current. At $x^* = -1$ m where the plunger occurred, significant energy components higher than, but not at,

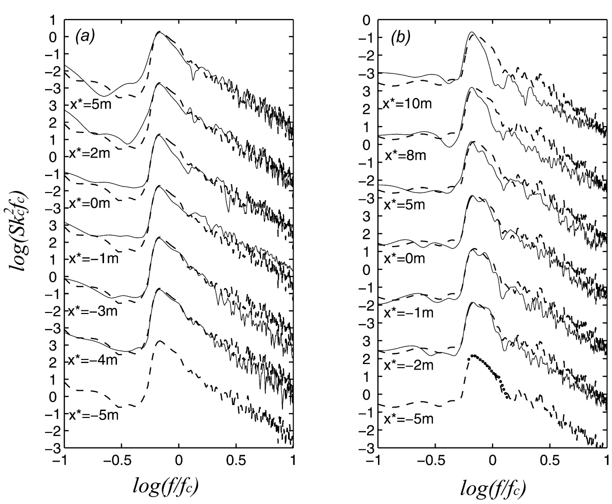

FIG. 10. Same in Fig. 9 but for (a) a plunger on a weak opposing current $U = -10$ cm s^{-1} in case 8 and (b) plunger on a strong opposing and current $U = -35$ cm s^{-1} in case 10.

the peak frequency, were lost. At the downstream $x^* = +5$ m, a relatively small amount of energy below the peak frequency was increased, indicating the energy gain from breaking, which will be further discussed in section 3d. Similar spatial evolution of the wave spectra was found in spilling breakers, with less energy dissipation and energy gain (not shown here). The above results raise a question regarding the occurrence of maximum dissipation. Donelan (1996) suggested that the spectral peak is the major energy flux balance between dissipation and wind input. From field data he showed that relatively higher dissipation at spectral peak exists for young wind seas under a strong wind forcing condition. For fully developed seas dissipation at the spectral peak gradually decreases. Therefore, we could hypothesize that without wind forcing in a paddle-generated wave field, little dissipation at the spectral peak would occur after breaking in focused wave groups, which is confirmed by the observations in Rapp and Melville (1990), Kway et al. (1998), Meza et al. (2000), and the present study.

Figure 10b shows the plunger on a strong opposing -35 cm s^{-1} current for case 10. In the comparison of the measured and the input spectra at $x^* = -5$ m, wave blocking slightly appeared in the range of frequencies higher than 1.1 Hz, consistent with the theoretical estimate using the kinematic conservation equation (Mei 1983). Because of the fact that close to the wave maker a slight decrease of opposing currents was found as the currents entered vertically to the setting tank via a bottom opening (Fig. 1), blocking was not clearly observed in the wave spectra until $x^* = -1$ m. As a result, wave reflection (Smith 1975; Shyu and Phillips 1990; Trulsen and Mei 1993) was expected to occur and led to the occurrence of high-frequency components, as shown in the frequency range between 1.1 and ~2.5 Hz in Fig. 10b. Interestingly, wave blocking somehow delayed the occurrence of the plunger to $x^* = 5$ m, where substantial energy dissipation above the spectral peak occurred. Meanwhile, a slight downshift of the spectral peak was visible at $x^* = 10$ m and maintained afterward. Similar spectral evolution, not shown here, was observed for case 9, with breaking on a partial wave blocking due to a weaker opposing current.

This permanent frequency downshifting after wave breaking on strong opposing currents contrasted the other experimental cases. For example, no frequency downshifting after breaking has been reported in relatively broadband-focused wave groups on a zero or weak current condition (Rapp and Melville 1990; Kway et al. 1998; Meza et al. 2000; Wu and Nepf 2002). On the other hand, wave breaking resulting from the sideband instability (Benjamin and Feir 1967) in narrowbanded wave trains has been shown to induce the permanent downshifting of the spectral peak (Melville 1982; Waseda and Tulin 1999). Permanent downshifting phenomenon was also found in other monochromatic and random breaking waves under full wave-blocking conditions (Lai et al. 1989; Chawla and Kirby 2002). Furthermore, Smith and Seabergh (2001) observed that the magnitude of permanent frequency downshifting depends on the strength of opposing currents that, in turn, reduce the frequency bandwidth of the wave. Combining the previous findings and our observation results, suggests that the permanent frequency downshifting would occur only for breaking in narrower wave trains.

Theoretical studies on the permanent frequency downshifting phenomenon in a unidirectional, nonlinear wave train have been conducted by many investigators, and well reviewed in Dias and Kharif (1999). Several mechanisms, including wave breaking (Trulsen and Dysthe 1990), wind forcing and eddy dissipation (Hara and Mei 1991), damping of the mean flow (Uchiyama and Kawahara 1994; Kato and Oikawaa 1995), and viscous dissipation and surface tension (Poitevin and Kharif 1991), have been shown to result in a permanent frequency downshifting. Interestingly, all of these theoretical studies are based upon the assumption of narrowbanded spectrum wave groups. Therefore, future research is needed to reveal the role of broad bandwidth of wave groups in permanent frequency downshifting due to wave breaking.

d. Energy gain and loss

The characteristics of energy loss higher than the peak frequency and energy gain below the peak frequency after breaking in the absence of current was first suggested by Melville (1996) and observed by Meza et al. (2000). For breaking in the presence of a current, a small amount of energy gain below the peak frequency was also identified in Fig. 10a. To further decipher these characteristics, the energy density spectra before and after plunger breakers were normalized with its peak spectral density S_p at the upstream reference position, as described in section 2c(2). Figure 11a shows the energy differences due to plungers in the present experiments. Overall, significant energy loss at the frequency components higher than the peak frequency $f/f_p = 1.0$–2.5, but not at the peak frequency, was clearly observed. Near and below the spectral peak frequency $f/f_p = 0.75$–1.0, a small amount of energy gain was noticeable. Specifically, the energy gain was considerably enhanced for partial wave-blocking conditions in cases 9 and 10, which may be caused by the peak frequency downshift. Similar patterns for spilling breakers were also seen in Fig. 11b, except for a smaller magnitude in comparison with plunging breakers. By integrating over corresponding frequency ranges, the ratio of total energy gain to total energy loss was obtained and summarized in Table 3. For example, the average gain-to-loss ratio for the plungers and spillers in cases 1–5 is 9% and 3%, respectively, consistent with the results in Meza et al. (2000). These ratios seem to vary with spectral frequency bandwidth. Higher ratios were observed for breakers on strong opposing currents with the partial

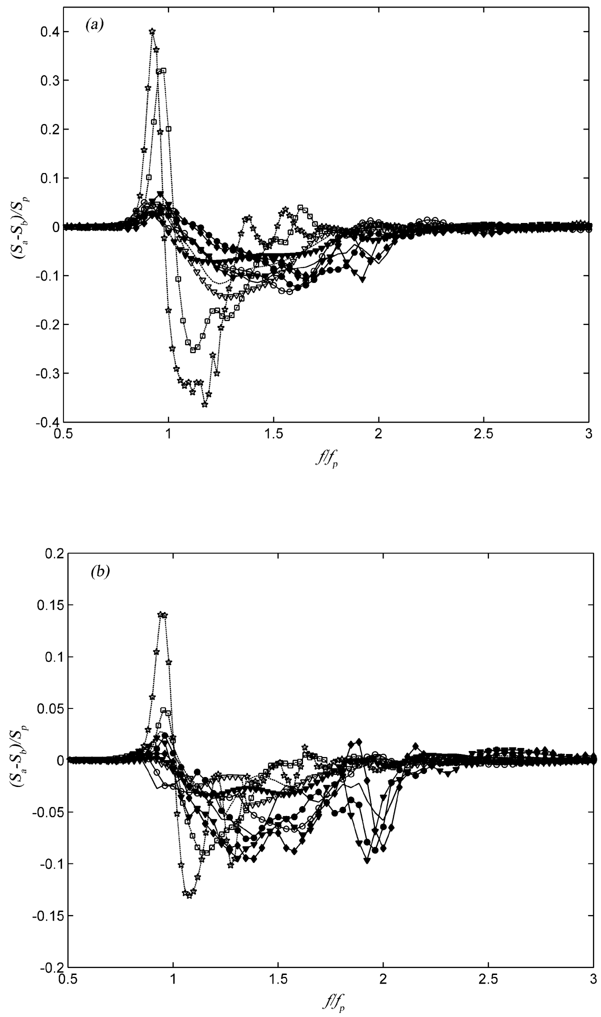

FIG. 11. Normalized differences in energy density spectra before (S_b) and after (S_a) a breaking event for (a) plungers and (b) spillers, with S_p the peak density: case 1 (solid line), case 2 (filled triangles on solid lines), case 3 (filled triangles on solid line), case 4 (filled diamonds on solid line), case 5 (open circles on solid line), case 6 (dash line), case 7 (filled circles on dash line), case 8 (open triangles on dash line), case 9 (open squares on dash line), and case 10 (open stars on dash line).

wave blocking. Further studies to address the energy gain-to-loss ratio dependence on spectral frequency bandwidth are needed.

4. Parameterizations of energy dissipation

a. Existing parameterizations

Operational wind-wave models for sea-state forecasting are generally based on the transport equation of the wave action density spectrum with sources of wind forcing, nonlinear wave–wave interactions, and energy dissipation due to breaking and bottom friction (Komen et al. 1994). Over several decades, extensive studies on the processes of wind forcing and nonlinear wave–wave

TABLE 3. Gain-to-loss ratio.

Case	Spectral bandwidth parameter ν	Gain-to-loss ratio	
		Spiller	Plunger
1	0.195	0.4	7.3
2	0.195	4.5	8.5
3	0.195	5.0	11.4
4	0.195	2.7	10.3
5	0.195	1.1	9.1
6	0.154	7.8	7.6
7	0.154	3.1	4.5
8	0.154	6.6	6.5
9	0.151	15.4	37.5
10	0.124	36.8	44.7

interactions have been made (Snyder et al. 1981; Janssen et al. 1989; Komen et al. 1994; Tolman and Chalikov 1996; Donelan 1999). For energy dissipation due to breaking, several spectral parameterizations of dissipation rates were also proposed and tested, including the most recent one by Henrique et al. (2003). In the following, we briefly describe the formulations of these dissipations in the context of a two-dimensional wave field and frequency spectra $S(\omega)$ derived from the time series of surface displacement measurements.

Based on the quasi-linear model (Hasselmann 1974; Komen et al. 1984), an improved parameterization of energy dissipation was proposed by Janssen et al. (1989) for the ocean wave prediction model (WAM), given by

$$D^{\mathrm{WAM}}(\omega) = C_{\mathrm{dis}}^{\mathrm{WAM}}\left(\frac{\hat{\alpha}}{\hat{\alpha}^{\mathrm{SP}}}\right)^{q_1}\left[(1-\delta)\left(\frac{\sigma}{\overline{\sigma}}\right)^2 + \delta\left(\frac{\sigma}{\overline{\sigma}}\right)^4\right]^{q_2/2} \times \overline{\varpi}S(\omega), \tag{14}$$

where the coefficient $C_{\mathrm{dis}}^{\mathrm{WAM}}$ and the exponents q_1 and q_2 are determined by fitting observation data; $\hat{\alpha} = m_0\overline{\varpi}^4/g^2$ is a spectral steepness parameter with m_0 the zeroth moment of the wave spectrum in Eq. (12), and $\overline{\varpi}$ is the mean apparent wave frequency; $\hat{\alpha}^{\mathrm{SP}}$ is an integrated steepness of a fully developed spectrum; and the kernel $[(1-\delta)(\sigma/\overline{\sigma})^2 + \delta(\sigma/\overline{\sigma})^4]^{q_2/2}$ controls the spectral distribution of energy dissipation with respect to the mean intrinsic wave frequency $\overline{\sigma}$. The default setup of WAM cycle 3 (WAMDI Group 1988) is $\delta = 0$, $q_1 = 2$, and $q_2 = 2$; the WAM cycle-4 (Janssen et al. 1989) model has $\delta = 0.5$, $q_1 = 2$, and $q_2 = 1$.

In recent years, the importance of breaking onset processes of wave groups has been recognized and incorporated into the parameterization of dissipation. For example, Chawla and Kirby (2002) proposed a dissipation formula as

$$D^{\mathrm{CK}}(\omega) = C_{\mathrm{dis}}^{\mathrm{CK}}\left(\frac{\sigma}{\overline{\sigma}}\right)^4 \overline{\varpi}S(\omega), \tag{15}$$

where $C_{\mathrm{dis}}^{\mathrm{CK}} = \langle D\rangle/\,\overline{\varpi}\int S(\omega)(\sigma/\overline{\sigma})^4\,d\omega$ is a nondimensional coefficient and $\langle D\rangle$, the total energy dissipation of all random wave components, is determined by experimental data with the consideration of a geometric steepness breaking criterion and breaking probability. In the present experiment, $\langle D \rangle$ was determined from the energy density spectra difference before and after a single breaking event. A more comprehensive and flexible spectral energy dissipation parameterization form, proposed by Henrique et al. (2003), is

$$D^{\mathrm{HAB}}(\omega) = C_{\mathrm{dis}}^{\mathrm{HAB}}(E_{\mathrm{tot}}k_p^2)^{h_1}\left(\frac{\sigma}{\overline{\sigma}}\right)^{2h_2}\left[\frac{B(\sigma)}{B_r}\right]^{h_3/2}\overline{\omega}S(\omega), \tag{16}$$

where $E_{\mathrm{tot}}k_p^2$ is an integral spectral steepness parameter, k_p^2 is the peak wavenumber, and a weighting function $(\sigma/\overline{\sigma})$ collectively accounts for mechanisms causing breaking and enhanced wave energy dissipations due to long wave–short wave and wave–turbulence interactions; B_r is the threshold saturation level, and $B(\sigma) = \sigma^5 S(\sigma)/2g^2$ is a local saturation parameter that can address the threshold behavior of the breaking wave contribution to dissipation, relative to the dissipation due to wave–turbulence interaction and straining of shorter waves (Banner et al. 2002); the exponent $h_3 = h_0/2 + h_0/2 \tanh\langle 10\{[B(\sigma)/B_r]^{1/2} - 1\}\rangle$ is set to 0 when $B(\sigma) < B_r$; and $C_{\mathrm{dis}}^{\mathrm{HAB}}$, h_0, h_1, and h_2 are the fitting coefficients.

b. *Proposed spectral parameterization*

The results in section 3 suggest that spectral evolution due to breaking has the following two main characteristics: 1) a threshold behavior of breaking onset and 2) significant energy dissipations at higher frequencies and small energy gain at lower frequencies, with respect to the spectral peak. To include these features, we modify the dissipation form, in analogy to Eq. (16), as

$$D(\omega) = C_{\mathrm{dis}}\left[\frac{\varepsilon_p}{(\varepsilon_p)_c}\right]^{r_1}\left(\frac{|\sigma - \sigma_p|}{\sigma_p}\right)^{r_2}\overline{\omega}S(\omega), \tag{17}$$

where C_{dis} is a nondimensional coefficient with $C_{\mathrm{dis}} = -C_1$ for $\omega > \omega_p$ and $C_{\mathrm{dis}} = \beta C_1$ for $\omega \leq \omega_p$, where C_1 is a positive nondimensional coefficient, and β is the total energy gain-to-loss ratio (section 3d); ε_p is the significant spectral peak steepness at the upstream reference position and $(\varepsilon_p)_c$ is the critical value of ε_p at the breaking onset that determines when dissipation is to be switched on; $[(|\sigma - \sigma_p|)/\sigma_p]$ controls the spectral distribution of energy dissipation, which delineates the intrinsic frequency range into two parts: (i) below the spectral peak frequency σ_p the expression leads to energy gain (positive D) and (ii) above spectral peak frequencies the distribution results in energy loss (negative D); $S(\omega)$ is the wave energy density spectrum before breaking, that is, at the upstream reference position, and r_1 and r_2 are the fitting coefficients.

The rationale to use significant spectral peak steepness ε_p in Eq. (17) lies in its dependence on the nondimensional spectral bandwidth parameter υ observed in the experiments. In Fig. 12, a strong correlation between $(\varepsilon_p)_c$ and υ, calculated by Eq. (11), for the onset of the incipient wave was found, indicating the important role of the slope of high wave frequency components and frequency bandwidth on the onset of breaking in a nonlinear wave group. Similar relationships also appeared in the spillers and plungers. In cases 6–8, the wave groups of a linear steepness wave spectrum have smaller υ than those of a constant steepness wave spectrum in cases 1–5, though all have the same frequency bandwidth $\Delta f/f_c$. Observations indeed showed that the $(\varepsilon_p)_c$ for the onset of breaking corresponding to cases 6–8 was elevated, suggesting that wave groups based upon a narrower-banded spectrum have higher critical $(\varepsilon_p)_c$. Considerably higher $(\varepsilon_p)_c$ appeared in cases 9–10, in which wave blocking reduced the frequency bandwidth and υ. Based upon these results, we believe that the dependence of $(\varepsilon_p)_c$ on υ of a wave group can provide a valuable role to address the threshold behavior of breaking-wave contribution to dissipation.

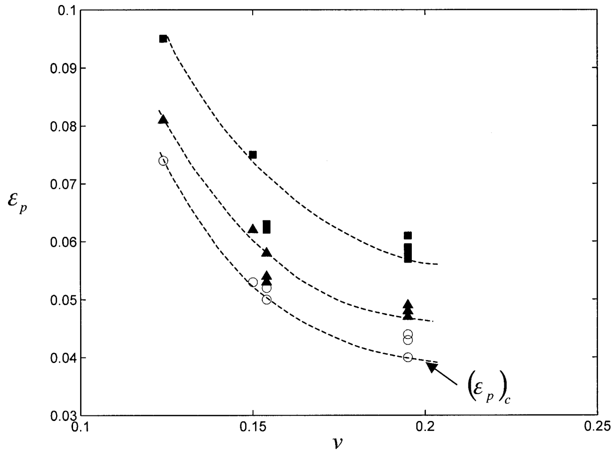

FIG. 12. Significant spectral peak steepness ε_p against the spectral bandwidth parameter υ for plungers (squares), spillers (triangles), and incipient waves (open circles).

c. *Comparison of model results and measurements*

The spectral energy dissipation through wave breaking in the experiment is defined as

$$D^M(\omega) = \frac{\Delta S(\omega)}{T_b}, \tag{18}$$

where $\Delta S(\omega)$ is the density spectral difference before and after wave breaking (chosen at the upstream and downstream reference positions), and T_b is a time scale for a single breaking event within a wave group. Normalizing Eq. (18) by the mean angular apparent frequency $\overline{\omega}$ and the spectral peak density S_p before breaking gives

$$\frac{D^M(\omega)}{\overline{\omega}S_p} \approx \frac{D^M(\omega)T_b}{S_p} = \frac{\Delta S(\omega)}{S_p}, \tag{19}$$

which is readily available in section 3d. Normalization

TABLE 4. Coefficients and exponents in five spectral parameterizations.

Model	Coefficients
WAM cycle 3	$q_1 = 2$ $q_2 = 2$ $C_{dis}^{WAM} = -8.33 \times 10^{-4}$ to -1.14×10^{-2} $\hat{\alpha}^{SP} = 1 \times 10^{-3}$ to 4×10^{-3}
WAM cycle 4	$m = 2$ $n = 1$–3 $\delta = 0.1$–0.3 $C_{dis}^{WAM} = -1.2 \times 10^{-3}$ to -5.1×10^{-3} $\hat{\alpha}^{SP} = 1 \times 10^{-3}$ to 4×10^{-3}
Chawla and Kirby (2002)	$C_{dis}^{CK} = -0.04$ to -0.22
Henrique et al. (2003)	$h_0 = 2$–4 $h_1 = 0$ $h_2 = 1$–2 $C_{dis}^{HAB} = -0.08$ to -0.2 $B_r = 2 \times 10^{-3}$ to 5×10^{-3}
The proposed formula	$r_1 = 2$ $r_2 = 1$ $C_1 = 0.5$–0.9

of the model spectral energy dissipation in Eqs. (14), (15), (16), and (17) was done in a similar manner. Careful fitting and sensitivity tests were performed to obtain best matches between the model results and measurements. Table 4 lists the fitting parameters and exponents used in five spectral dissipation formulas.

Comparisons between measurements and the model results using Eqs. (14), (15), (16), and (17) are shown in Fig. 13. For nonblocking plunger and spiller cases in Figs. 13a–d all models can simulate the measured significant energy dissipation at higher-frequency components fairly well. Nevertheless, the feature of a small energy gain at lower-frequency components cannot be modeled except for using the proposed formula in Eq. (17). In particular, for the wave-blocking case the $[(|\sigma - \sigma_p|)/\sigma_p]$ in the proposed formula provides a mechanism to account for the energy gain up to 30% below $f/f_p = 1.0$ in Fig. 13e and 13f. However, below the theoretical blockage frequency (Mei 1983) $f/f_p = 1.8$, the results from the proposed model overpredicted the measured dissipations. This discrepancy may result from the possibility of energy pile up below the blockage frequency, which was also observed by Huang et al. (1972), Smith and Seabergh (2001), and Chawla and Kirby (2002). This energy pile up below the blockage frequency, however, was better simulated using more flexible models like the WAM cycle-4 formula ($\delta = 0.1$ and $q_2 = 1$) and Henrique et al.'s parameterization ($B_r = 0.005$ and $h_2 = 1$).

5. Summaries and recommendations

In this study, we investigated the energy dissipation by unsteady wave breaking on currents in a laboratory flume. Based upon the concept of wave–wave and wave–current interactions, an isolated breaker within a wave group was generated by focusing wave components at one location at a specified time. We extended this focusing method in a wave field on strong opposing currents that are able to block partial high-frequency components of waves. Experimental cases of various wave conditions, including a range of current conditions (bidirection and strength), wave spectrum slopes (linear or constant), and breaking intensities (incipient, spiller, and plunger waves) were conducted. The goal of this study was to examine loss of excess energy flux and spectral distribution of energy dissipation before and after a single breaker. Several findings from this study are summarized as follows:

1) The mean spectral slope $\overline{dS^*/df^*}$ play an important role in determining the loss of excess energy flux due to breaking. Diverse energy losses of wave breaking from the present and previous experimental studies (Rapp and Melville 1990; Lamarre 1993; Kway et al. 1998) have been reconciled and clarified. In general, a steeper $\overline{dS^*/df^*}$ yields less energy loss. The spectrum mean slope is believed to be closely associated with the equilibrium range of wave spectra in fully developed wind seas.
2) For breaking in the presence and absence of currents, two characteristics regarding the spectral distribution of energy dissipation were identified: (a) significant energy dissipation occurred at frequency components that were higher than the spectral peak frequency, and little change at the peak frequency was found; and (b) a small energy gain was observed at lower-frequency components.
3) A threshold behavior of the onset of deep water breaking on currents was found. Two spectral parameters, a critical significant spectral peak steepness $(\varepsilon_p)_c$, and a spectral bandwidth parameter υ were identified, supporting the relevance of nonlinear wave group dynamics to wave breaking (Banner and Tian 1998; Banner et al. 2000, 2002). Reduction in υ of a wave group due to partial wave blocking leads to steeper waves at breaking onset, indicating the significance of interplay between wave–current and wave–wave interactions.
4) The proposed spectral energy dissipation parameterization of breaking on currents incorporated the threshold behavior of breaking onset and spectral distribution of the energy gain–loss behavior. Partial wave blocking in a strong opposing current was taken into account in the spectral parameterization. Overall, model predictions of the spectral energy dissipation were found to be in good agreement with experimental measurements.

While some findings of the energy dissipation from unsteady breakers on currents were revealed in this study, future work on this subject should include

1) understanding the cause of energy gain at the lower spectral components below the peak frequency,
2) investigating the effects of frequency bandwidth on

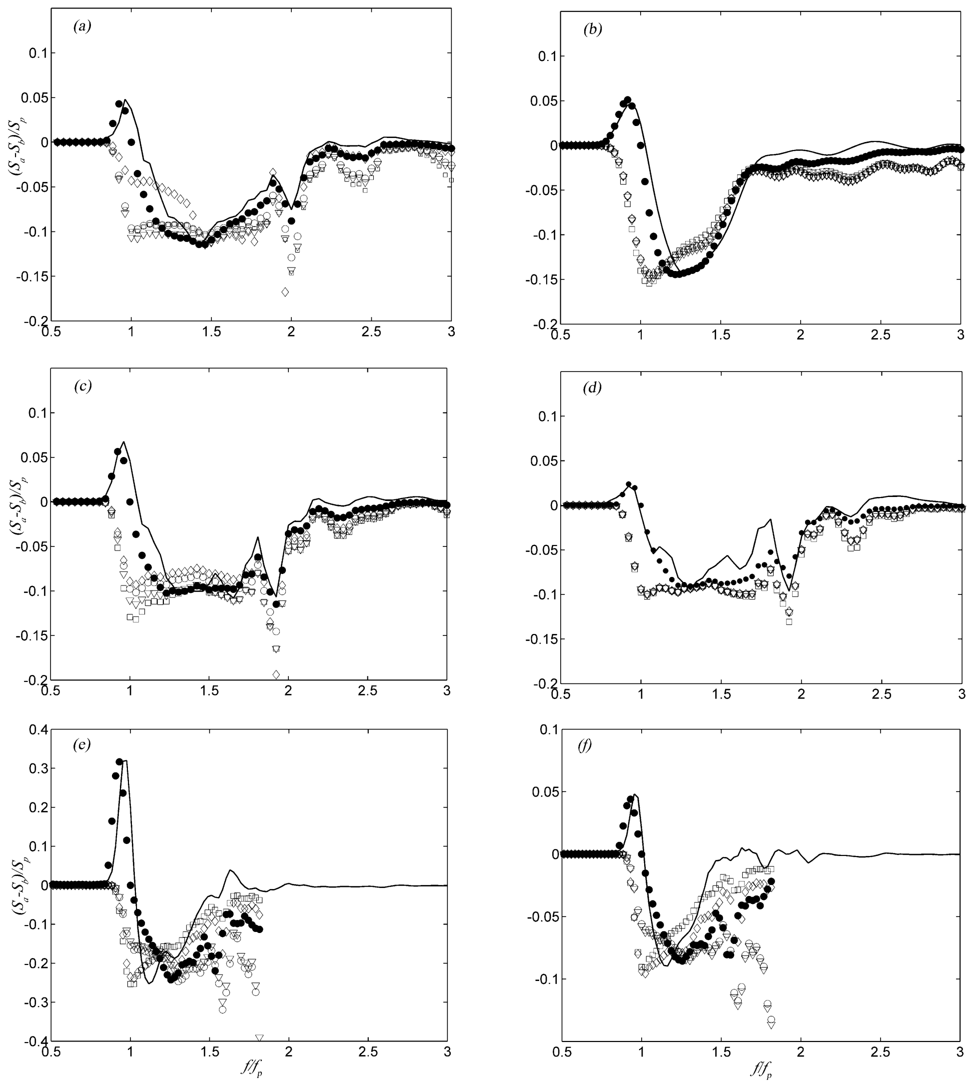

FIG. 13. Comparison of spectral distribution of wave energy dissipation between the various model predictions and experimental measurements in (a) case-1 plunger, (b) case-8 plunger, (c) case-3 plunger, (d) case-3 spiller, (e) case-9 plunger, and (f) case-9 spiller. In each plot, the solid lines are measurements; the proposed form (filled circles), Chawla and Kirby (2002; open circles), Henrique et al. (2003; open diamonds), WAM cycle 3 (open triangles), and WAM cycle 4 (open square) represent the various model results.

peak frequency downshifting due to wave blocking or wave breaking in a nonlinear wave group,

3) assessing the performance of proposed parameterizations and other models under a wider range of field conditions, and
4) examining the effects of wave directionality (She et al. 1997; Wu and Nepf 2002; Henrique et al. 2003) and shear currents (Swan et al. 2001; Banner and Song 2002; Banner et al. 2002) on the threshold behavior of breaking onset within a nonlinear wave group, and these two effects on spectral energy dissipations due to breaking.

Acknowledgments. The authors gratefully acknowledge the support from the U.S. Office of Naval Research, the Wisconsin Alumni Research Foundation, and the College of Engineering at UW—Madison. The authors specifically thank Dr. James B. Edson at the Woods Hole Oceanographic Institution for valuable advice.

REFERENCES

Alber, I. E., 1978: The effects of randomness on the stability of two-dimensional wavetrains. *Proc. Roy. Soc. London Ser. A,* **363,** 525–546.

Baldock, T. E., C. Swan, and P. H. Taylor, 1996: A laboratory study of nonlinear surface waves on water. *Philos. Trans. Roy. Soc. London,* **A452,** 649–676.

Banner, M. L., and O. M. Phillips, 1974: On the incipient breaking of small-scale waves. *J. Fluid Mech.,* **65,** 647–656.

——, and D. H. Peregrine, 1993: Wave breaking in deep-water. *Annu. Rev. Fluid Mech.,* **25,** 373–397.

——, and X. Tian, 1998: On the determination of the onset of wave breaking for modulating surface gravity water waves. *J. Fluid Mech.,* **367,** 107–137.

——, J. B. Song, 2002: On determining the onset and strength of breaking for deep water waves. Part II: Influence of wind forcing and surface shear. *J. Phys. Oceanogr.,* **32,** 2559–2570.

——, A. V. Babanin, and I. P. Young, 2000: Breaking probability for dominant waves on the sea surface. *J. Phys. Oceanogr.,* **30,** 3145–3160.

——, J. R. Gemmrich, and D. M. Farmer, 2002: Multiscale measurements of ocean wave breaking probability. *J. Phys. Oceanogr.,* **32,** 3364–3375.

Benjamin, T., and J. Feir, 1967: The disintegration of wave trains in deep water. *J. Fluid Mech.,* **27,** 373–397.

Booij, N., R. C. Ris, and L. H. Holthuijsen, 1999: A third generation wave model for coastal regions. Part 1. Model description and validation. *J. Geophys. Res.,* **104,** 7649–7666.

Brown, M. G., and A. Jensen, 2001: Experiments on focusing unidirectional water waves. *J Geophys. Res.,* **106,** 16 917–16 928.

Chawla, A., and J. T. Kirby, 1998: Experimental study of wave breaking and blocking on opposing currents. *Proc. 26th Int. Conf. on Coastal Engineering,* Copenhagen, Denmark, ASCE, 759–772.

——, and ——, 2002: Monochromatic and random wave breaking at blocking points. *J. Geophys. Res.,* **107,** 3067, doi:10.1029/2001/JC001042.

Dias, F., and C. Kharif, 1999: Nonlinear gravity and capillary-gravity waves. *Annu. Rev. Fluid Mech.,* **31,** 301–345.

Dold, J. W., and D. H. Peregrine, 1986: Water-wave modulations. Vol. 1, *Proc. 20th Int. Conf. on Coastal Engineering,* Taipei, Taiwan, ASCE, 163–175.

Donelan, M. A., 1996: Air-water exchange processes. *Physical Processes in Lakes and Oceans,* J. Imberge, Ed., Vol. 54, *Coastal and Estuarine Studies,* Amer. Geophys. Union, 19–36.

——, 1999: Wind-induced growth and attenuation of laboratory waves. *Wind-Over-Wave Couplings: Perspectives and Prospects,* S. G. Sajjadi et al., Eds., University of Salford, 183–194.

——, and Y. Yuan, 1999: Wave dissipation by surface processes. *Dynamics and Modeling of Ocean Waves,* G. J. Komen et al., Eds., Cambridge University Press, 143–155.

——, M. S. Longuet-Higgins, and J. S. Turner, 1972: Periodicity in whitecaps. *Nature,* **239,** 449–451.

Duncan, J., 1981: An experimental investigation of breaking waves produced by a towed hydrofoil. *Proc. Roy. Soc. London,* **377A,** 331–348.

——, 2001: Spilling breakers. *Annu. Rev. Fluid Mech.,* **33,** 519–547.

Hara, T., and C. C. Mei, 1991: Frequency downshift in narrowbanded surface waves under the influence of wind. *J. Fluid Mech.,* **230,** 429–477.

Hasselmann, K., 1962: On the non-linear transfer in a gravity wave spectrum, Part 1: General theory. *J. Fluid Mech.,* **12,** 481–500.

——, 1974: On the spectral dissipation of ocean waves due to white-capping. *Bound.-Layer Meteor.,* **6,** 107–127.

Hedges, T. S., K. Anastasiou, and D. Gabriel, 1985: Interaction of random waves and currents. *J. Waterw. Port Coastal Ocean Eng. Amer. Soc. Civ. Eng.,* **111,** 275–288.

Henrique, J., G. M. Alves, and M. Banner, 2003: Performance of a saturation-based dissipation-rate source term in modeling the fetch-limited evolution of wind waves. *J. Phys. Oceanogr.,* **33,** 1274–1298.

Holthuijsen, L. H., and T. H. C. Herbers, 1986: Statistics of breaking waves observed as whitecaps in the open sea. *J. Phys. Oceanogr.,* **16,** 290–297.

Huang, N. E., 1986: An estimate of the influence of breaking waves on the dynamics of the upper ocean. *Wave Dynamics and Radio Probing of the Sea Surface,* O. M. Phillips and K. Hasselmann, Eds., Plenum, 295–313.

——, D. T. Chen, C.-C. Tung, and J. R. Smith, 1972: Interactions between steady non-uniform currents and gravity waves with applications for current measurements. *J. Phys. Oceanogr.,* **2,** 420–431.

Janssen, P. A. E. M., P. Lionelle, M. Reistad, and A. Hollingsworth, 1989: Hindcasts and data assimilation studies with the WAM model during the Seasat period. *J. Geophys. Res.,* **94C,** 973–993.

Johannessen, T. B., and C. Swan, 2001: A laboratory study of the focusing of transient and directionally spread surface water waves. *Philos. Trans. Roy. Soc. London,* **A457,** 971–1006.

Jonsson, I. G., 1990: Wave current interactions. *The Sea,* J. Wiley and Sons, B. LeMehaute and D. M. Hanes, *Ocean Engineering Science,* Vol. 9, 65–120.

Kato, Y., and M. Oikawa, 1995: Wave number downshift in modulated wavetrain through a nonlinear damping effect. *J. Phys. Soc. Japan,* **64,** 4660–4669.

Kemp, P. H., and R. R. Simons, 1982: The interaction between waves and a turbulent current-waves propagating with current. *J. Fluid Mech.,* **116,** 227–250.

——, and ——, 1983: The interaction between waves and a turbulent current-waves propagating against current. *J. Fluid Mech.,* **130,** 73–89.

Kjeldsen, S. P., and D. Myrhaug, 1979: Breaking waves in deep waters and resulting forces. *Proc. 11th Offshore Technology Conf.,* Houston, TX, OTC, Paper 3646.

Komen, G. J., K. Hasselmann, and S. Hasselmann, 1984: On the existence of a fully developed wind-sea spectrum. *J. Phys. Oceanogr.,* **14,** 1271–1285.

——, L. Cavaleri, M. Donelan, K. Hasselmann, S. Hasselmann, and P. A. E. M. Janssen, 1994: *Dynamics and Modeling of Ocean Waves.* Cambridge University Press, 532 pp.

Kway, J. H. L., Y. S. Loh, and E. S. Chan, 1998: Laboratory study of deep-water breaking waves. *Ocean Eng.,* **25,** 657–676.

Lai, R. J., S. R. Long, and N. E. Huang, 1989: Laboratory studies of wave-current interaction: Kinematics of the strong interaction. *J. Geophys. Res.,* **94,** 16 201–16 214.

Lamarre, E., 1993: An experimental study of air entrainment by breaking waves. Ph.D. thesis, Massachusetts Institute of Technology, 327 pp.

Longuet-Higgins, M. S., 1969: A nonlinear mechanism for generation of sea waves. *Proc. Roy. Soc. London,* **177,** 293–306.

——, 1984: Statistical properties of wave group in a random sea state. *Philos. Trans. Roy. Soc. London Ser. A Math. Phys. Sci.,* **312,** 219–250.

——, and R. W. Stewart, 1960: Changes in the form of short gravity waves on long waves and tidal currents. *J. Fluid Mech.,* **8,** 565–583.

Mei, C. C., 1983: *The Applied Dynamics of Ocean Surface Waves.* John Wiley & Sons, 740 pp.

Melsom, A., 1996: Effects of wave breaking on the surface drift. *J. Geophys. Res.,* **101,** 12 071–12 078.

Melville, W. K., 1982: The instability and breaking of deep-water waves. *J. Fluid Mech.,* **115,** 165–185.

——, 1994: Energy dissipation by breaking waves. *J. Phys. Oceanogr.,* **24,** 2041–2049.

——, 1996: Wave breaking in air-sea interaction. *Annu. Rev. Fluid Mech.,* **28,** 279–321.

——, and R. J. Rapp, 1985: Momentum flux in breaking waves. *Nature,* **317,** 514–516.

Meza, E., J. Zhang, and R. J. Seymour, 2000: Free-wave energy dissipation in experimental breaking waves. *J. Phys. Oceanogr.,* **30,** 2404–2418.

Nepf, H. M., C. H. Wu, and E. S. Chan, 1998: A comparison of two- and three-dimensional wave breaking. *J. Phys. Oceanogr.,* **28,** 1496–1510.

Peirson, W. L., A. W. Garcia, and S. E., Pells, 2003: Water wave attenuation due to opposing wind. *J. Fluid Mech.,* **487,** 345–365.

Pelinovsky, E., and C. Kharif, 2000: Simplified model of the freak wave formation from the random wave field. *Proc. 15th Int.*

Workshop on Water Waves and Floating Bodies, Caesaria, Israel, IWWWFB, 142–145.

Peregrine, D. H., 1976: Interaction of water waves and currents. *Adv. Appl. Mech.,* **16,** 9–117.

Phillips, O. M., 1977: *The Dynamics of the Upper Ocean.* Cambridge University Press, 336 pp.

——, 1984: On the response of short ocean wave components at a fixed wavenumber to ocean current variation. *J. Phys. Oceanogr.,* **14,** 1425–1433.

——, 1985: Spectral and statistical properties of the equilibrium range in wind-generated gravity waves. *J. Fluid Mech.,* **156,** 505–531.

Poitevin, J., and C. Kharif, 1991: Subharmonic transition of a nonlinear wave train on deep water. *Mathematical and Numerical Aspects of Wave Propagation Phenomena,* G. C. Cohen, L. Halpern, and P. Joly, Eds., SIAM, 567–576.

Rapp, R. J., and W. K. Melville, 1990: Laboratory measurements of deep water breaking waves. *Phil. Trans. Roy. Soc. London,* **A331,** 735–780.

Resio, D. T., 1987: Shallow-water waves, I: Theory. *J. Waterw. Port Coastal Ocean Eng.,* **113,** 264–281.

Ris, R. C., and L. H. Holthuijsen, 1996: Spectral modeling of current induced wave-blocking. *Proc. 25th Coastal Engineering Conf.,* Orlando, FL, ASCE, 1247–1254.

Rosengaus-Moshinsky, M., 1987: Experimental study of wave-generated bedforms and resulting wave attenuation. Ph.D. thesis, Massachusetts Institute of Technology, 279 pp.

Schneggenburger, C., H. Gunther, and W. Rosenthal, 2000: Spectral wave modeling with nonlinear dissipation: Validation and application in a coastal tidal environment. *Coastal Eng.,* **41,** 201–235.

She, K., C. A. Greated, and W. J. Easson, 1997: Experimental study of three-dimensional wave breaking. *J. Waterw. Port Coastal Ocean Eng. Amer. Soc. Civ. Eng.,* **120,** 20–36.

Shyu, J. H., and O. M. Phillips, 1990: The blockage of gravity and capillary waves by longer waves and currents. *J. Fluid Mech.,* **217,** 115–141.

Slunyaev, A., C. Kharif, E. Pelinovsky, and T. Talipova, 2002: Nonlinear wave focusing on water of finite depth. *Physica D,* **173,** 77–96.

Smith, J. M., and W. C. Seabergh, 2001: Wave breaking on a current at an idealized inlet with an ebb shoal. U.S. Army Corps of Engineers, Waterways Experimental Station Tech. Rep. ERDC/CHL TR-01-7, 31 pp.

Smith, R., 1975: Reflection of short gravity waves on a non-uniform current. *Math. Proc. Cambridge Philos. Soc.,* **78,** 517–525.

Snyder, R. L., F. W. Dobson, J. A. Elliott, and R. B. Long, 1981: Array measurements of atmospheric pressure fluctuations above surface gravity waves. *J. Fluid Mech.,* **102,** 1–59.

Su, M. Y., M. Bergin, P. Marler, and R. Myrick, 1982: Experiments on nonlinear instabilities and evolution of steep gravity-wave trains. *J. Fluid Mech.,* **124,** 45–72.

Suh, K. D., Y. Y. Kim, and D. Y. Lee, 1994: Equilibrium-range spectra of waves propagating on currents. *J. Waterw. Port Coastal Ocean Eng. Amer. Soc. Civ. Eng.,* **120,** 434–450.

——, S. H. Oh, S. W. Thurston, and N. Hashimoto, 2000: Influence of currents on equilibrium range spectra of wind waves. *J. Waterw. Port Coastal Ocean Eng. Amer. Soc. Civ. Eng.,* **126,** 79–87.

Swan, C., I. P. Cummins, and R. L. James, 2001: An experimental study of two-dimensional surface water waves propagating on depth-varying currents. Part 1. Regular waves. *J. Fluid Mech.,* **428,** 273–304.

Teixeira, M. A. C., and S. E. Belcher, 2002: On the distortion of turbulence by a progressive surface wave. *J. Fluid Mech.,* **458,** 229–267.

Terray, E. A., M. A. Donelan, Y. C. Agrawal, W. M. Drennan, K. K. Kahma, S. A. Kitaigorodskii, P. A. Hwang, and A. J. Williams, 1996: Estimates of kinetic energy dissipation under breaking waves. *J. Phys. Oceanogr.,* **26,** 792–807.

Thais, L., and J. Magnaudet, 1996: Turbulent structure beneath surface gravity waves sheared by the wind. *J. Fluid Mech.,* **328,** 313–344.

——, G. Chapalain, G. Klopman, R. R. Simons and G. P. Thomas, 2001: Estimates of wave decay rates in the presence of turbulent currents. *Appl. Ocean Res.,* **23,** 125–137.

Thomas, G. P., and G. Klopman, 1997: Wave-current interactions in the nearshore region. *Gravity Waves in Water of Finite Depth,* J. N. Hunt, Ed., Computational Mechanics Publications, 215–319.

Tolman, H. L., and D. Chalikov, 1996: Source terms in a third-generation wind wave model. *J. Phys. Oceanogr.,* **26,** 2497–2518.

Trulsen, K., and K. B. Dysthe, 1990: Frequency downshift through self-modulation and breaking. *Water Wave Kinematics,* A. Tørum and O. T. Gudmestad, Eds., Kluwer, 561–572.

——, and C. C. Mei, 1993: Double reflection of capillary gravity-waves by a non-uniform current—A boundary-layer theory. *J. Fluid Mech.,* **251,** 239–271.

Uchiyama, Y., and T. Kawahara, 1994: A possible mechanism for frequency down-shift in nonlinear wave modulation. *Wave Motion,* **20,** 99–110.

WAMDI Group, 1988: The WAM model—A third generation ocean wave prediction model. *J. Phys. Oceanogr.,* **18,** 1775–1810.

Waseda, T., and M. P. Tulin, 1999: Experimental study of the stability of deep-water wave trains including wind effects. *J. Fluid Mech.,* **401,** 55–84.

Wu, C. H., and H. Nepf, 2002: Breaking criteria and energy losses for three-dimensional wave breaking. *J. Geophys. Res.,* **107,** 3177, doi:10.1029/2001JC001077.